Tunable Thickness and Photoluminescence of Bipyramidal Hexagonal β-$NaYF_4$ Microdisks

Jianle Zhuang,[†] Jing Wang,[†] Xianfeng Yang,[†] Ian D. Williams,[‡] Wei Zhang,[†] Qinyuan Zhang,[§] Zhouming Feng,[§] Zhongmin Yang,[§] Chaolun Liang,[†] Mingmei Wu,*[,†] and Qiang Su[†]

MOE Key Laboratory of Bioinorganic and Synthetic Chemistry/State Key Laboratory of Optoelectronic Materials and Technologies, School of Chemistry and Chemical Engineering, Instrumental Analysis and Research Center, Sun Yat-Sen (Zhongshan) University, Guangzhou 510275, P. R. China, Department of Chemistry, Hong Kong University of Science and Technology, Clear Water Bay, Kowloon, Hong Kong, P. R. China, and MOE Key Laboratory of Specially Functional Materials and Institute of Optical Communication Materials, South China University of Technology, Guangzhou 510640, P. R. China

Received September 18, 2008. Revised Manuscript Received October 28, 2008

Hexagonal β-$NaYF_4$ was synthesized as capped bipyramidal microdisks solvothermally from yttria (Y_2O_3), sodium fluoride and ammonium hydrogen fluoride. The microdisks are bound by up to eighteen faces; six $\{20\bar{2}3\}$ facets on both the top and bottom of the disk and six radial $\{10\bar{1}0\}$ facets around its central band. The overall morphology and particle size can be modified through change of temperature or alcoholic solvent, both of which affect the development of the $\{10\bar{1}0\}$ faces. The photoluminescence properties of doped microdisks, such as down-conversion in the case of β-$NaYF_4$:Eu^{3+} or up-conversion for β-$NaYF_4$:Yb^{3+}/Er^{3+}, were investigated in detail. The lifetime and emission of the Eu^{3+} and Er^{3+} ions appear related to the morphology of the host crystals. This system provides an excellent example in the tuning and optimization of the optical properties of a material through morphological control via facile change of synthetic conditions.

Introduction

The synthesis of inorganic materials with morphological control has attracted a great deal of interest for its potential applications in optoelectronics, information technology, catalysis, and sensing.[1−4] The properties of a material can be greatly affected not only by its chemical composition and crystal structure, but also by its form, and in the case of microcrystalline powders by the particle size and shape. Much endeavor has been made to tune the properties of materials through synthetic modification of their size and shape.[5,6] Among this numerous research, most of these efforts have been focused on the tunability of optical property of semiconductors and metals due to the tunable bandgap and surface plasmon resonance (SPR).[2,7] For anisotropic semiconducting and metal nanocrystals, chemical adsorption, and heterogeneous catalysis, as well as physical absorption and emission spectra, are related to the growth direction and the crystal surface structure.[2,8] That is, the properties of these crystalline materials can be varied by tuning the aspect ratios for rodlike and disk-like geometries. Recently, both micro- and nanosized rare-earth photoluminescence materials have been attracting considerable attention.[9,10] In particular, the size-related down- and up-conversion emissions for such

* Corresponding author. E-mail: ceswmm@mail.sysu.edu.cn.
[†] Sun Yat-Sen (Zhongshan) University.
[‡] Hong Kong University of Science and Technology.
[§] South China University of Technology.

(1) (a) Xia, Y. N.; Yang, P. D.; Sun, Y. G.; Wu, Y. Y.; Mayers, B.; Gates, B.; Yin, Y. D.; Kim, F.; Yan, Y. Q. *Adv. Mater.* **2003**, *15*, 353. (b) Xiong, Y. J.; Mayers, B. T.; Xia, Y. N. Chem. Commun. 2005, *5013*. (c) Purkayastha, A.; Lupo, F.; Kim, S.; Borca-Tasciuc, T.; Ramanath, G. *Adv. Mater.* **2006**, *18*, 496.
(2) Qu, L. H.; Peng, X. G. *J. Am. Chem. Soc.* **2002**, *124*, 2049.
(3) (a) Tian, N.; Zhou, Z. Y.; Sun, S. G.; Ding, Y.; Wang, Z. L. *Science* **2007**, *316*, 732. (b) Xiong, Y. J.; Xie, Y.; Li, Z. Q.; Li, X. X.; Gao, S. M. *Chem.—Eur. J.* **2004**, *10*, 654.
(4) (a) Liang, H. P.; Lawrence, N. S.; Jones, T. G. J.; Banks, C. E.; Ducati, C. *J. Am. Chem. Soc.* **2007**, *129*, 6068. (b) Battaglia, D.; Peng, X. G. *Nano Lett.* **2002**, *2*, 1027.
(5) (a) Burda, C.; Chen, X. B.; Narayanan, R.; El-Sayed, M. A. *Chem. Rev.* **2005**, *105*, 1025. (b) Wang, M.; Huang, Q. L.; Hong, J. M.; Chen, X. T.; Xue, Z. L. *Cryst. Growth Des.* **2006**, *6*, 2169. (c) Han, J. T.; Huang, Y. H.; Wu, X. J.; Wu, C. L.; Wei, W.; Peng, B.; Huang, W.; Goodenough, J. B. *Adv. Mater.* **2006**, *18*, 2145. (d) Yang, J.; Li, C. X.; Zhang, X. M.; Quan, Z. W.; Zhang, C. M.; Li, H. Y.; Lin, J. *Chem.—Eur. J.* **2008**, *14*, 4336.
(6) (a) El-Sayed, M. A. *Acc. Chem. Res.* **2004**, *37*, 326. (b) Yan, Q. Y.; Purkayastha, A.; Kim, T.; Kroger, R.; Bose, A.; Ramanath, G. *Adv. Mater.* **2006**, *18*, 2569.
(7) (a) Wang, Q. B.; Seo, D. K. *Chem. Mater.* **2006**, *18*, 5764. (b) Xiong, H. M.; Liu, D. P.; Xia, Y. Y.; Chen, J. S. *Chem. Mater.* **2005**, *17*, 3062. (c) Xiong, Y. J.; Wiley, B.; Chen, J. Y.; Li, Z. Y.; Yin, Y. D.; Xia, Y. N. *Angew. Chem., Int. Ed.* **2005**, *44*, 7913. (d) Yu, H.; Li, J. B.; Loomis, R. A.; Gibbons, P. C.; Wang, L. W.; Buhro, W. E. *J. Am. Chem. Soc.* **2003**, *125*, 16168.
(8) (a) Lee, S. M.; Cho, S. N.; Cheon, J. *Adv. Mater.* **2003**, *15*, 441. (b) Yu, H.; Li, J. B.; Loomis, R. A.; Wang, L. W.; Buhro, W. E. *Nat. Mater.* **2003**, *2*, 517. (c) Tian, Z. R. R.; Voigt, J. A.; Liu, J.; McKenzie, B.; McDermott, M. J.; Rodriguez, M. A.; Konishi, H.; Xu, H. F. *Nat. Mater.* **2003**, *2*, 821. (d) Kuykendall, T.; Pauzauskie, P. J.; Zhang, Y. F.; Goldberger, J.; Sirbuly, D.; Denlinger, J.; Yang, P. D. *Nat. Mater.* **2004**, *3*, 524.
(9) (a) Wang, X.; Li, Y. D. *Chem.—Eur. J.* **2003**, *9*, 5627. (b) Si, R.; Zhang, Y. W.; You, L. P.; Yan, C. H. *Angew. Chem., Int. Ed.* **2005**, *44*, 3256. (c) Wang, X.; Li, Y. D. *Angew. Chem., Int. Ed.* **2003**, *42*, 3497. (d) Wang, M.; Huang, Q. L.; Zhong, H. X.; Chen, X. T.; Xue, Z. L.; You, X. Z. *Cryst. Growth Des.* **2007**, *7*, 2106.
(10) (a) Goldys, E. M.; Drozdowicz-Tomsia, K.; Sun, J. J.; Dosev, D.; Kennedy, I. M.; Yatsunenko, S.; Godlewski, M. *J. Am. Chem. Soc.* **2006**, *128*, 14498. (b) Yan, R. X.; Li, Y. D. *Adv. Funct. Mater.* **2005**, *15*, 763. (c) Yi, G. S.; Chow, G. M. *J. Mater. Chem.* **2005**, *15*, 4460.

10.1021/cm802543k CCC: $40.75
Published on Web 12/04/2008

materials have been extensively studied and found to be affected by the surface defects.[10]

Up-conversion (UC) phosphors, which can convert lower energy to higher energy, have a long history in the fields of solid-state lasers, low-intensity IR imaging, NIR (near-infrared) quantum counting devices, 3D flat-panel displays, and biological labels.[11−28] Among the various UC phosphors, $NaYF_4$ has been one of the most efficient UC phosphor hosts,[12−28] and in particular, hexagonal β-$NaYF_4$, which has been found to be much more efficient than its cubic α-polymorph.[13−15] In the last 5 years, growing attention has been paid to the wet chemistry synthesis of $NaYF_4$ crystals. A variety of wet chemistry routes have been developed for the fabrication of $NaYF_4$ crystals. α-$NaYF_4$ nanoparticles were synthesized by coprecipitation at room temperature.[16] More recently, high-quality β-$NaYF_4$ nanodisks were grown via thermal decomposition of lanthanide trifluoroacetate precursors in oleic acid/oleyamine/1-octadecene (OA/OL/ODE) system by several research groups.[17,18] However, it requires high temperature (at 330 °C) to obtain phase-pure β-$NaYF_4$ nanodisks and the byproducts are considered to be toxic. It was indicated that α-$NaYF_4$ is the kinetic product and precipitates first in such synthetic routes, with progressive phase transformation to the thermodynamically stable β-$NaYF_4$ phase under further heat treatment.[13,14,24−26] Consequently, the complete precipitation of β-$NaYF_4$ from initially as-formed α-nanocrystals requires quite forcing conditions. Due to the long aging times and high temperature required the product crystals are typically nonuniform due to Oswald ripening. Many recent reports demonstrate that α-$NaYF_4$ exists as intermediate product of β-$NaYF_4$ and much endeavor has been made to the quick and facile formation of β-$NaYF_4$.[13,14,24−26] Kinetically, the key issue is to make a more facile wet growth of β-$NaYF_4$ crystals by either reducing the activation energy for the transformation of α-$NaYF_4$ to β-$NaYF_4$ or through avoidance of the initial formation of α-$NaYF_4$.[17,26]

Previously uniform crystals of β-$NaYF_4$ were generally grown in a homogeneous solution phase system using soluble inorganic or organic yttrium salts as precursor. A simple route using ethanol as solvent was reported to synthesize slightly irregular β-$NaYF_4$ nanoparticles,[22] however, these products exhibit gray body color and their UC efficiency was significantly reduced. Herein, we present a simple and economical route to synthesize bipyramidal hexagonal microdisks of β-$NaYF_4$ in a heterogeneous (solid-solution) reaction system, using the simple reactants ytrria (Y_2O_3), sodium fluoride (NaF), ammonium hydrogen fluoride (NH_4HF_2), and a variety of alcohols under solvothermal conditions. That the system affords phase pure β-$NaYF_4$ with no evidence for the intermediate formation of α-$NaYF_4$ as a kinetic product is unprecedented. Variation of the synthetic conditions allows a high degree of morphological control over the disk-like product microcrystals, principally through change in the development of radial $\{10\bar{1}0\}$ faces. The photoluminescence properties of the related Ln doped products have been investigated and it appears that the luminescent lifetime and UC properties of Ln-doped β-$NaYF_4$ can be monotonously tuned along with the crystal morphology.

Experimental Section

Chemicals. All chemicals were commercially available and were used as received without further purification. Rare earth oxides were supplied by Guangdong Zhujiang Rare Earths Co., Ltd., China. NaF, NH_4HF_2, methanol, isopropanol, ethanol, *n*-butanol, *n*-hexanol, acetic acid, and ethylamine were purchased from Guangzhou Chemical Reagent Factory, China. Particular attention should be paid to the safe use of these organic solvents while carrying out a solvothermal synthesis because they are flammable, corrosive, irritant and/or toxic liquids.

Solvothermal Synthesis. In a typical synthesis, solid Y_2O_3 (0.25 mmol), NaF (1.5 mmol) and NH_4HF_2 (6.0 mmol, excess) were mixed directly in a 23 mL Teflon-cup. Ten milliliters of an alcohol such as ethanol was then added as solvent. After vigorous magnetic stirring for ca. 30 min, the Teflon-lined autoclave was tightly sealed and heated to 140−220 °C for different time periods. The autoclave was then cooled down to ambient temperature and the solid products were washed several times alternately with ethanol and distilled water. Other solvents such as *n*-butanol, *n*-hexanol, water, acetic acid, or ethylamine were also used instead of ethanol for comparison while keeping other reaction conditions unchanged.

Characterization. The solid products were characterized using powder X-ray diffraction (Rigaku D/MAX 2200 VPC) at a scanning rate of 10°/min, with Cu Kα radiation (λ = 0.1541 nm). The

(11) (a) Auzel, F. *Chem. Rev.* **2004**, *104*, 139. (b) Suyver, J. F.; Aebischer, A.; Biner, D.; Gerner, P.; Grimm, J.; Heer, S.; Kramer, K. W.; Reinhard, C.; Gudel, H. U. *Opt. Mater.* **2005**, *27*, 1111. (c) Sivakumar, S.; van Veggel, F. C. J. M.; May, P. S. *J. Am. Chem. Soc.* **2007**, *129*, 620. (d) Gerner, P.; Reinhard, C.; Gudel, H. U. *Chem.—Eur. J.* **2004**, *10*, 4735. (e) Sivakumar, S.; Diamente, P. R.; van Veggel, F. C. *Chem.—Eur. J.* **2006**, *12*, 5878. (f) Sivakumar, R.; van Veggel, F. C. J. M.; Raudsepp, M. *J. Am. Chem. Soc.* **2005**, *127*, 12464.
(12) (a) Zhang, F.; Wan, Y.; Yu, T.; Zhang, F. Q.; Shi, Y. F.; Xie, S. H.; Li, Y. G.; Xu, L.; Tu, B.; Zhao, D. Y. *Angew. Chem., Int. Ed.* **2007**, *46*, 7976. (b) Mai, H. X.; Zhang, Y. W.; Sun, L. D.; Yan, C. H. *J. Phys. Chem. C* **2007**, *111*, 13730. (c) Chen, G. Y.; Liu, Y.; Zhang, Y. G.; Somesfalean, G.; Zhang, Z. G.; Sun, Q.; Wang, F. P. *Appl. Phys. Lett.* **2007**, *91*, 133103. (d) Li, Z. Q.; Zhang, Y. *Angew. Chem., Int. Ed.* **2006**, *45*, 7732. (e) Wang, L.; Li, Y. Chem. Commun. 2006, *2557*. (f) Sun, Y. J.; Chen, Y.; Tian, L. J.; Yu, Y.; Kong, X. G.; Zhao, J. W.; Zhang, H. *Nanotechnology* **2007**, *18*, 275609. (g) Wang, L. Y.; Li, Y. D. *Chem. Mater.* **2007**, *19*, 727. (h) Su, Y. G.; Li, L. P.; Li, G. S. *Cryst. Growth Des.* **2008**, *8*, 2678.
(13) Zhuang, J. L.; Liang, L. F.; Sung, H. H. Y.; Yang, X. F.; Wu, M. M.; Williams, I. D.; Feng, S. H.; Su, Q. *Inorg. Chem.* **2007**, *46*, 5404.
(14) Wang, L. Y.; Yan, R. X.; Hao, Z. Y.; Wang, L.; Zeng, J. H.; Bao, H.; Wang, X.; Peng, Q.; Li, Y. D. *Angew. Chem., Int. Ed.* **2005**, *44*, 6054.
(15) Kramer, K. W.; Biner, D.; Frei, G.; Gudel, H. U.; Hehlen, M. P.; Luthi, S. R. *Chem. Mater.* **2004**, *16*, 1244.
(16) Yi, G. S.; Lu, H. C.; Zhao, S. Y.; Yue, G.; Yang, W. J.; Chen, D. P.; Guo, L. H. *Nano Lett.* **2004**, *4*, 2191.
(17) Mai, H.-X.; Zhang, Y.-W.; Si, R.; Yan, Z.-G.; Sun, L.-d.; You, L.-P.; Yan, C.-H. *J. Am. Chem. Soc.* **2006**, *128*, 6426.
(18) (a) Boyer, J.-C.; Vetrone, F.; Cuccia, L. A.; Capobianco, J. A. *J. Am. Chem. Soc.* **2006**, *128*, 7444. (b) Boyer, J. C.; Cuccia, L. A.; Capobianco, J. A. *Nano Lett.* **2007**, *7*, 847.
(19) Mai, H. X.; Zhang, Y. W.; Sun, L. D.; Yan, C. H. *J. Phys. Chem. C* **2007**, *111*, 13721.
(20) Heer, S.; Kompe, K.; Gudel, H. U.; Haase, M. *Adv. Mater.* **2004**, *16*, 2102.
(21) Wang, L. Y.; Li, Y. D. *Nano Lett.* **2006**, *6*, 1645.
(22) Zeng, J. H.; Su, J.; Li, Z. H.; Yan, R. X.; Li, Y. D. *Adv. Mater.* **2005**, *17*, 2119.
(23) Li, C. X.; Quan, Z. W.; Yang, J.; Yang, P. P.; Lin, J. *Inorg. Chem.* **2007**, *46*, 6329.
(24) Li, C. X.; Yang, J.; Quan, Z. W.; Yang, P. P.; Kong, D. Y.; Lin, J. *Chem. Mater.* **2007**, *19*, 4933.
(25) Yi, G. S.; Chow, G. M. *Adv. Funct. Mater.* **2006**, *16*, 2324.
(26) Shan, J. N.; Ju, Y. G. *Appl. Phys. Lett.* **2007**, *91*, 123103.
(27) Liang, X.; Wang, X.; Zhuang, J.; Peng, Q.; Li, Y. D. *Adv. Funct. Mater.* **2007**, *17*, 2757.
(28) Wang, Z. J.; Tao, F.; Yao, L. Z.; Cai, W. L.; Li, X. G. *J. Cryst. Growth* **2006**, *290*, 296.

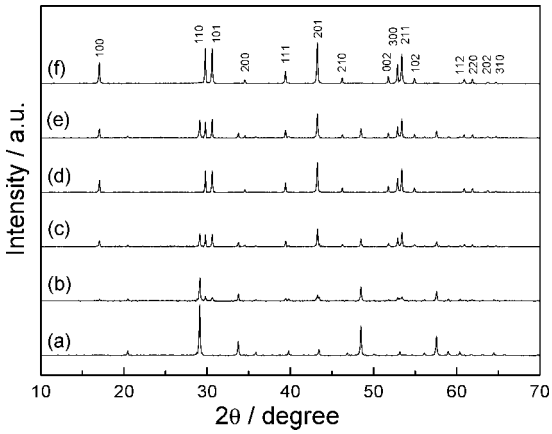

Figure 1. Power XRD patterns of (a) commercial Y_2O_3 starting reagent and isolated products synthesized in ethanol at 140 °C for (b) 5, (c) 10, and (d) 24 h and 220 °C for (e) 1 and (f) 3 h. The indexing in (f) is for hexagonal β-$NaYF_4$, based on JCPDS card 16−0334.

morphology of the as-prepared particles was observed using scanning electron microscopy (SEM, FEI Quanta 400). Transmission electron microscopy (TEM) and selected area electron diffraction (SAED) analyses were performed on a JEOL 2010 high-resolution transmission electron microscope equipped with an Oxford Instruments EDS system. Down-conversion luminescence spectra were measured on a Fluorolog-3 spectrofluorometer (Jobin Yvon Inc./Specx) equipped with a 450 W Xe lamp, double excitation monochromators and single emission monochromator. Up-conversion emission spectra were detected by the same instrument equipped with an external 980 nm diode laser and a R928P photomultiplier tube. The room-temperature (RT) lifetime measurements were determined on a FSP920-combined time-resolved and steady-state fluorescence spectrometer (Edinburgh Instruments) equipped with a μF900 microsecond flash lamp.

Results and Discussion

Effect of Reaction Temperature and Time. The powder X-ray diffraction (pXRD) patterns of products from ethanol at 140 and 220 °C and different times are shown in Figure 1 along with that of the commercial Y_2O_3 used as reagent. Figure 1b−d show progress of the reaction at 140 °C after 5, 10, and 24 h respectively and indicate mixtures of Y_2O_3 and β-$NaYF_4$ with increasing product formation over time. After 24 h β-$NaYF_4$ is found to be the exclusive product. Panels e and f in Figure 1 show the progress after 1 and 3 h, respectively, at 220 °C. As anticipated the reaction rate is accelerated by increasing reaction temperature[13,17] so that the β-$NaYF_4$ product is phase pure after 3 h.

By contrast with previous studies there is no evidence of intermediary formation of α-$NaYF_4$.[13,14,17,24] In this respect, our experimental results in which β-$NaYF_4$ could be directly grown from solid Y_2O_3 precursor through a solution chemistry are quite unique.

In the pXRD patterns, the relative intensities of the 001 diffraction peaks are enhanced versus h00 compared to the prismatic β-$NaYF_4$ samples we had previously prepared,[13] implying the growth along the *c*-axis is inhibited and the aspect ratios (hexagonal prism length to thickness) is reduced. In order to confirm this SEM was conducted on the solid products and the representative results are shown in Figure 2. The starting material, Y_2O_3, is composed of irregular grains, each of which is assembled by nanoparticles (Figure 2a and the Supporting Information, Figure S1). In the solvothermal reaction system at 140 °C, the initial Y_2O_3 nanoparticles are found to be dispersed and gradually replaced by an increasing number of β-$NaYF_4$ microdisks of approximately 2 μm diameter (Figure 2a−d). At initial reaction stage, as in our previous work,[13] β-$NaYF_4$ crystals grow quickly after nucleation. During the further reaction up to ca. 24 h, Y_2O_3 grains gradually disappear and the disks tend to be thicker and wider. However, the geometric outline preserves as the early grown ones (images c and d in Figure 2). Each of the clamlike microcrystals with a clear crevice around the center edge, i.e. the baseline, looks to be stacked by several thinner nanodisks (Figure 2d).

Although electron microscopy analysis indicates that the dimensions of these disks changed negligibly during "growth stage" at a specific reaction temperature, the thickness of the microdisks increases significantly at a higher growth temperature (Figure 2d−f). Higher-temperature (such as 180 and 220 °C) leads to the growth of well-defined disks with smooth outer surfaces (images e and f in Figure 2). With increasing the reaction temperature, the crevices around the center lines disappear and facets later shown to be $\{10\bar{1}0\}$ with increasing thicknesses tend to be more significant (Figures 2d−f). When temperature reaches 220 °C, the "disk" becomes thicker with obvious side facets of ca. 250 nm (Figure 2f). However, the size and the outer geometry of each pair of pyramidal caps remain with negligible variation. That is the diameters of the disks are essentially almost identical among Figures 2d−f, regardless of the reaction temperatures. The above experimental results suggest that the reaction temperature has obvious effects on the thickness of the platy bases but not on the geometry of the pyramidal caps.

As illustrated in Figure 2d−f, although the growth habit varies from the formation of hexagonal bipyramids to bipyramid-capped disks, the vertex angle of the ideal projecting triangle of a hexagonal pyramid is constant and all of these crystals can be considered to possess D_{6h} point symmetry. Figure 3a shows the TEM image of the disk projected along the $[1\bar{2}10]$ direction. The angle at the vertex is measured as 131°, which is in good agreement with the calculated value (130.98°) between two opposite $\{20\bar{2}3\}$ facets. This result suggests that the cap of a disk is bounded by twelve $\{20\bar{2}3\}$ facets, such a polyhedral geometry of β-$NaYF_4$ crystals is quite unique and has not been reported before. The idealized model of the crystal in Figure 3a is schematically illustrated in models b and c in Figure 3, viewed along the $[1\bar{2}10]$ and $[10\bar{1}0]$ directions respectively. Because the caps of the hexagonal disks are formed by twelve equivalent $\{20\bar{2}3\}$ facets, the parameters making the variation in the geometry of a disk are only attributed to thickness (*H*) and width (*W*) (Figure 3c). The thickness of the disk is enhanced at higher temperature as seen in Figure 2d−f. This indicates a lower differential rate of growth perpendicular to the $\{20\bar{2}3\}$ and $\{10\bar{1}0\}$ planes as the temperature is increased.

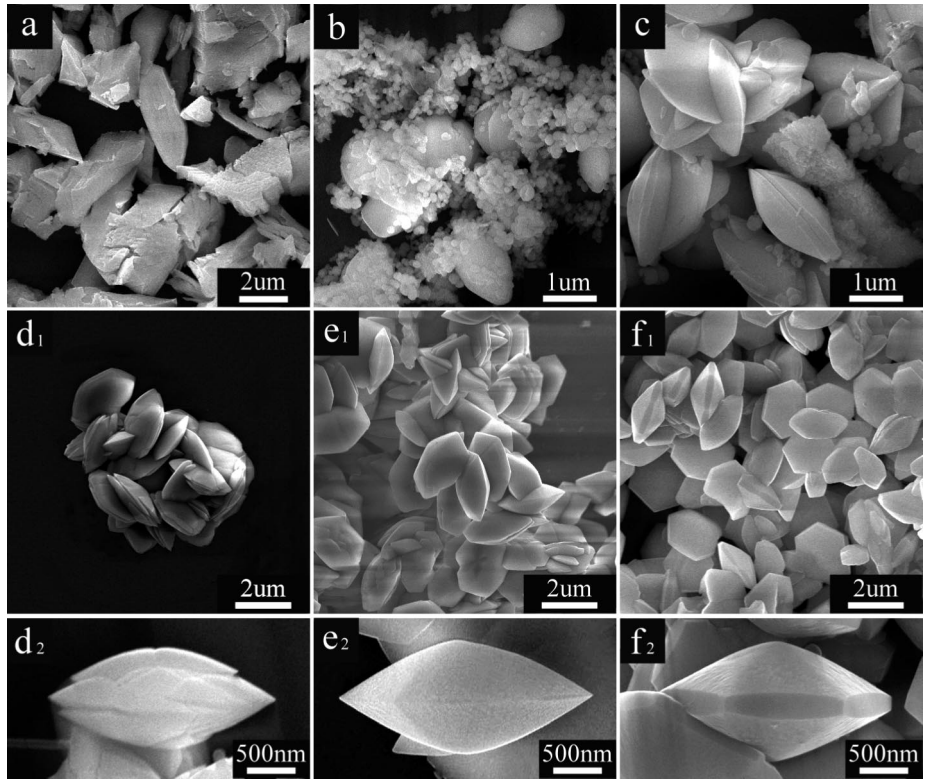

Figure 2. SEM images of (a) commercial Y_2O_3 and products synthesized in ethanol at 140 °C for (b) 5, (c) 10, and (d) 24 h, and at (e) 180 °C for 24 h and (f) 220 °C for 24 h.

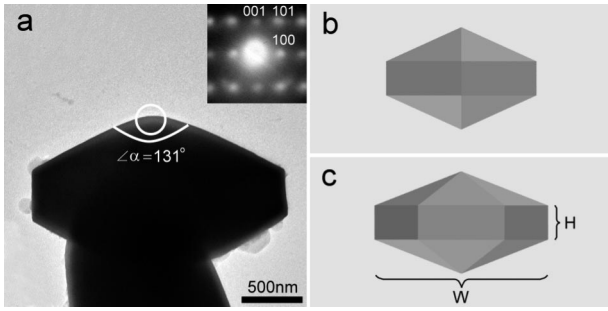

Figure 3. (a) TEM image of a β-$NaYF_4$ crystal taken along the $[1\bar{2}10]$ direction. Insert shows the corresponding SAED pattern. (b) Schematic model of the crystal viewed along $[1\bar{2}10]$. (c) Schematic model of the crystal viewed along $[10\bar{1}0]$, showing the thickness (*H*) and width (*W*).

Effect of Reaction Medium. In the above section we have described how morphologically controlled phase-pure β-$NaYF_4$ has been directly grown from oxide precursor in ethanol solvent. If the solvent is changed to water, acetic acid, or even ethylamine, the powder XRD patterns indicate that β-$NaYF_4$ is also produced, though reaction is incomplete even at 220 °C for 24 h (see the Supporting Information, Figure S2). Instead, mixtures of precursory Y_2O_3 and resultant β-$NaYF_4$ were detected. In the same case as in ethanol, α-$NaYF_4$ phase did not appear during the entire growth procedure according to the powder XRD patterns, indicative of direct conversion of Y_2O_3 to β-$NaYF_4$ irrespective of whichever solvent is used. These results suggest that the use of the yttria precursor, Y_2O_3, may play a crucial role in the direct nucleation and growth of β-$NaYF_4$. On the basis of the percent conversion and quality of the product powder XRD patterns (see the Supporting Information, Figure S2), the sequence of ethanol > acetic acid > $H_2O \gg$ ethylamine is found in effecting the overall conversion of yttria to the fluoride product. The fundamental reason why ethanol can better facilitate the growth of β-$NaYF_4$ than these other solvents is still under exploration.

Apart from ethanol, we have found that other *n*-alcohols such as *n*-butanol and *n*-hexanol could also be used as solvent to effect the formation of β-$NaYF_4$ from Y_2O_3. Figure 4a−c show the SEM images of β-$NaYF_4$ microdisks grown at 220 °C for 24 h from ethanol, *n*-butanol, and *n*-hexanol, respectively. These SEM images reveal an interesting result: the crystal shape changes from the bicapped disks to bicapped drums when the reaction medium changes from ethanol to *n*-hexanol, because the $\{10\bar{1}0\}$ facets are expanded, whereas the shape of the caps remains essentially the same. Both the *H* and *W* values of these crystals tend to be larger with the increase of alkyl-chain of alcohol but the increase in *H*, and thus the aspect ratio, changes substantially as seen by SEM micrographs (Figure 4 and the Supporting Information, Figure S3). For all three alcohols, the vertex angle of each pyramidal cap is identical indicating preservation of the capping facets in each case. The experimental results that "the longer the alkyl-chain, the larger the size, thickness, and aspect ratio" was also observed when the reaction temperature varied, such as at 180 °C (see the Supporting Information, Figure S4), implying that the solvent favors the growth of β-$NaYF_4$ crystals in the sequence *n*-hexanol > *n*-butanol > ethanol. Phase pure β-$NaYF_4$ was unable to be obtained when methanol was used as a solvent (see the Supporting Information, Figure S5), which fits in with the sequence that the growth of β-$NaYF_4$ is less favored in an alcohol with a short alkyl-chain. In addition, hexagonal

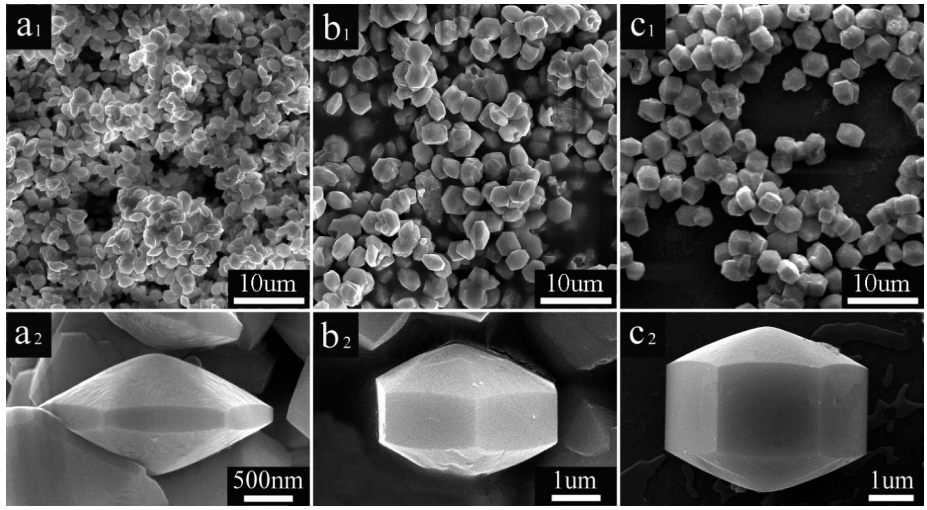

Figure 4. SEM images of β-$NaYF_4$ synthesized at 220 °C for 24 h in different solvents: (a) ethanol, (b) *n*-butanol, and (c) *n*-hexanol.

microdisks of phase-pure β-$NaYF_4$ can also be grown in isopropanol, with a similar growth behavior as in that of ethanol (see the Supporting Information, Figure S6). These experimental observations indicate a better control of β-$NaYF_4$ crystals in both size and shape via this facile and simple solvothermal growth route. Previously, hydrothermally and solvothermally grown nano/micro-β-$NaYF_4$ crystals were generally found to exhibit rod-like structures with much higher aspect ratios.[13,21,28] Recently, β-$NaYF_4$ nanodisks have been grown from organic solvents[17,25] and microdisks from hydrothermal process using citrate as a polydentate ligands.[23,24] However, the possibility of monotonously controllable thickness and aspect ratios and the appearance of $\{20\bar{2}3\}$ facets for β-$NaYF_4$ are quite unique to this work.

Effect of Reactants. It has been reported that use of different fluoride sources can lead to different morphologies of $NaYF_4$.[24] The width of β-$NaYF_4$ rods have been modified by altering the NaF to Y mole ratio in reactions.[27] In our process, NH_4HF_2 apparently plays an important role in the direct formation of phase pure β-$NaYF_4$, since no $NaYF_4$ phase can be obtained if NaF was used as the only source of fluoride. Furthermore we have found that the mole ratio of NH_4HF_2 to Y^{3+} should be greater than 6:1 to obtain phase pure β-$NaYF_4$, although the mole ratio of 2:1 should be sufficient for the formation of phase-pure β-$NaYF_4$ based on stoichiometry. This is because oxide is used as reactant. As in many solvothermal processes involving relatively insoluble oxide phases such as silicates, fluoride acts as a mineralizer, acting to solubilize the oxide and thus enhancing the rate of product formation.[29]

In most previous studies, soluble inorganic or organometallic yttrium salts, such as yttrium nitrate and yttrium trifluoroacetate, were used as reagents instead of insoluble yttria.[13,14,17−19] Herein, if yttrium nitrate is used as the precursor in ethanol, β-$NaYF_4$ is formed, but as irregular nanoparticles rather than as regular microdisks (see the Supporting Information, Figure S7). In summary, all three solid reagents used, Y_2O_3, NaF and NH_4HF_2 play significant roles in the nucleation and growth of these regular β-$NaYF_4$ microcrystals with the specific morphologies described above.

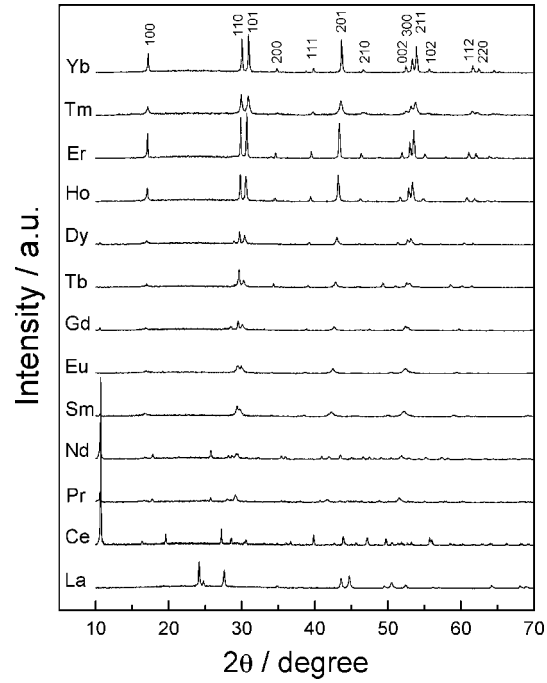

Figure 5. Powder XRD patterns of products synthesized from different rare earth oxides, NaF and excess NH_4HF_2 in ethanol at 180 °C for 24 h. All rare earth oxides used are Ln_2O_3 (Ln = La, Nd, Sm, Eu, Gd, Dy, Ho, Er, Tm, Yb) except for CeO_2, Pr_6O_{11}, and Tb_4O_7.

Extension to Other Related Rare Earth Fluorides. We have sought to extend this synthetic method to other related rare earth fluorides from their corresponding oxides, through reaction with NaF and NH_4HF_2. Figure 5 shows the pXRD patterns of the products synthesized from different rare earth oxides. The results may be categorized in several groups as follows. Group I for Lanthanum only, gave pure hexagonal LaF_3 at 180 °C for 24 h (Figure 5La). The SEM image (see the Supporting Information, Figure S8A-a) shows the product was composed of highly oriented nanodisks. The disk-like morphology of LaF_3 is very common and found in previous

(29) (a) Ivanova, S.; Louis, B.; Ledoux, M. J.; Pham-Huu, C. *J. Am. Chem. Soc.* **2007**, *129*, 3383. (b) Bull, I.; Villaescusa, L. A.; Teat, S. J.; Camblor, M. A.; Wright, P. A.; Lightfoot, P.; Morris, R. E. *J. Am. Chem. Soc.* **2000**, *122*, 7128. (c) Zones, S. I.; Darton, R. J.; Morris, R.; Hwang, S. J. *J. Phys. Chem. B* **2005**, *109*, 652.

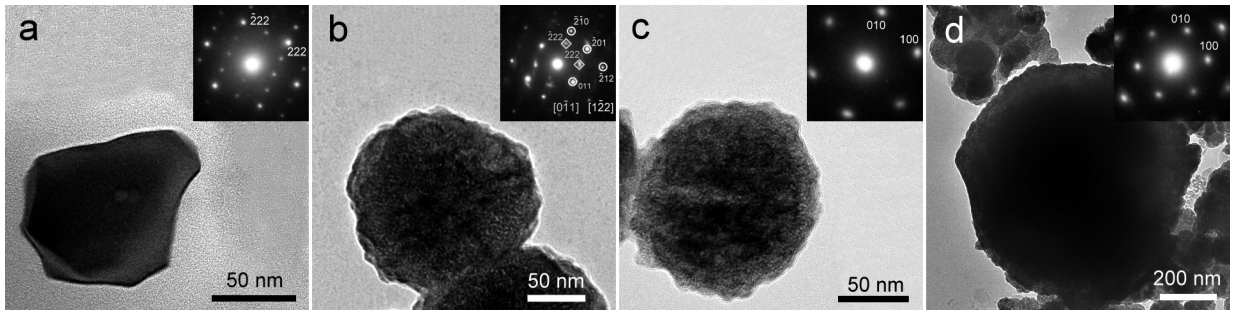

Figure 6. TEM images (a−d) and related selected area electron diffraction (SAED) patterns (insert) of (a) precursor Y_2O_3 grain, (b−d) some individual grains in the product as shown in either Figure 1b or Figure 2b with a mixture phase of Y_2O_3 and β-$NaYF_4$. The square and circle labeled spots in the insert of (b) correspond to Y_2O_3 and β-$NaYF_4$ with zone axes of [0$\bar{1}$1] and [1$\bar{2}$2], respectively. The grains in (c) or (d) are phase-pure β-$NaYF_4$, taken along the same zone axis of [001].

work in which LaF_3 was prepared solvothermally even in the presence of sodium and/or ammonium cations.[13,17,30] The second type of result, Group II with Ln = Ce gave tetragonal NH_4CeF_5 (Figure 5Ce and the Supporting Information, Figure S9, JCPDS card 19−0278). This was identified on the basis of its pXRD pattern in the powder diffraction database. It is of note that Ce(IV) can be preserved under these solvothermal conditions. The product of NH_4CeF_5 is a rare example of a Ce(IV) product grown via such an autoclaving chemistry. The third set of characteristic product types, group III, For Ln = Pr, Nd gave hexagonal NH_4LnF_4 as the major product, together with a minor amount of hexagonal β-$NaLnF_4$ (Pr and Nd spectra in Figure 5 and the Supporting Information, Figure S10). It was found previously that LnF_3 (Ln = Pr, Nd) was obtained hydrothermally by fluoridation when either $Ln(NO_3)_3$ or $LnCl_3$ was adopted as starting materials either in the presence or absence of sodium salt. [13,30] In the above four products, no cubic α-$NaLnF_4$ (Ln = La, Ce, Pr. or Nd) was detected according to the above powder XRD patterns (Figure 5Ln−Nd and the Supporting Information, Figure S9 and Figure S10). For the last group, i.e., group IV with relatively heavy rare earth elements, almost-phase-pure hexagonal $NaLnF_4$ (Ln = Sm−Yb) could be obtained via this oxide-precursor approach (Figure 5Sm−Yb). The intensities of 101 peaks tended to be enhanced as compared to those of 110, implying that the growth along *c*-directions is relatively reduced for these $NaLnF_4$ crystals containing heavier rare earth elements (Figure 5 and the Supporting Information, Figure S8). Typical SEM images of β-$NaLnF_4$ (Ln = Eu, Dy, Ho, and Er) crystals appearing as different morphologies ranging from hexagonal rods to hexagonal disks (see the Supporting Information, Figure S8Ab−e) support the evidence. The related powder XRD patterns for the samples grown at 220 °C show a similar phenomenon. The growth of β-$NaHoF_4$ and β-$NaErF_4$ was quite similar to that of $NaYF_4$ (see the Supporting Information, Figure S8Ad−f). There are also no corresponding cubic α-$NaLnF_4$ phases appearing during the solvothermal growth, implying that the β-$NaLnF_4$ (Ln = Sm−Yb) obtained here were synthesized directly from related rare-earth oxides in the series of these heavy rare earth elements. This result fits with the fact that the ionic radius of Y^{3+} (107.5 pm for 9-coordinate ion) lies in the middle of this series and is most similar to Ho^{3+} (107.2 pm).

Growth Mechanism. It has been well-accepted before that the kinetic product, i.e., α-$NaYF_4$, is formed as the intermediate phase at earlier solution growth stage and then transforms to the thermodynamically stable product, i.e. β-$NaYF_4$.[13,14,17,24] The kinetically precipitated α-$NaYF_4$ then transforms to hexagonal β-$NaYF_4$ polymorph through a redissolution and regrowth process.[13,17,24] That is, the growth of α-$NaYF_4$ is related to a LS (liquid to solid) mechanism, wherease that of β-$NaYF_4$ is related to a SLS [solid (redissolution of cubic polymorph) to liquid (mass transfer) to solid (renucleation and regrowth for hexagonal $NaYF_4$)] one. In general, because of a slow transformation from solid α-$NaYF_4$ to solid β-$NaYF_4$ on kinetic opinion, the as-grown α-$NaYF_4$ can be preserved for a much longer time and even phase-pure α-$NaYF_4$ can be readily obtained at a much lower reaction temperature and/or shorter reaction time. A good example is the previous growth of α-$NaYF_4$ nanocrystals in the mixed solvent of oleic acid and oleylamine.[17,18] On the other hand, nearly all of the recent reports about the growth of $NaYF_4$ have involved homogeneous reaction systems, i.e., the solid product is formed directly from solution phase. However, in this work, solid Y_2O_3 crystals have very low solubility in the alcohol solvent and the entire growth procedure is certainly attributed to heterogeneous reaction. With the addition of NH_4HF_2, the growth of hexagonal phase is facilitated. This might be attributed to an improved mass flux in the solvent system for the growth of hexagonal phase, i.e., the solubility of Y_2O_3 is highly enhanced with the addition of NH_4HF_2 in comparison to the lone addition of NaF. The formation of β-$NaYF_4$ is still based on an SLS process and it may be argued that insufficient aggregation of growth ions occurs to allow formation of the α-polymorph. From careful examination using TEM, we would propose that a topotactic growth mechanism may also be involved in which yttria grains may serve to nucleate the β-$NaYF_4$ product phase.

To investigate the growth process, typical nanocrystals of the precursor Y_2O_3, an intermediate mixed phase product containing both Y_2O_3 and β-$NaYF_4$, and of the final product, phase-pure β-$NaYF_4$, were examined in detail by TEM imaging and related SAED patterns, as well as by HRTEM imaging with related FFT patterns (see Figure 6, and the

(30) Liang, X.; Wang, X.; Wang, L. Y.; Yan, R. X.; Peng, Q.; Li, Y. D. *Eur. J. Inorg. Chem.* **2006**, 2186.

Supporting Information, Figures S11 and S12). Figure 6a shows a TEM image of a larger precursor Y_2O_3 single crystal separated ultrasonically from an aggregate (see the Supporting Information, Figure S1). The SAED pattern (Figure 6a, insert) indicates it is a single crystal with zone axis of $[0\bar{1}1]$. More structural characterizations such as X-ray diffraction (Figure 1a) and electron microscopy (see the Supporting Information, Figure S11 and S12a) confirm its high crystalline quality. Figure 6b is a TEM image of a grain isolated from a product obtained in ethanol at 140 °C for 5 h (Figure 2b). The related SAED pattern of the entire individual grain shows two sets of diffraction spots, the sharp ones labeled in circles are from β-$NaYF_4$, indicative of a single crystal nature, whereas the more diffuse ones arise from Y_2O_3, indicating that a possible strain in the Y_2O_3 lattice has been induced during its fluoridation. It can be found that there are deep pores all over the entire grain as shown in Figure 6b, which were not observed in the Y_2O_3 single crystal as shown in Figure 6a. These pores are assumed to arise from dissolution of the yttria in some specific spots facilitated by the etching of NH_4HF_2.

The TEM image and the SAED pattern with single-crystal-like but combined two sets of electron diffractions as shown in Figure 6b taken along the zone axes of $[1\bar{2}2]_{NYF}$ (subscript of NYF denoted as β-$NaYF_4$) and of $[0\bar{1}1]_{YO}$ (subscript YO denoted as Y_2O_3) suggests a possible corresponding orientation between them. According to the indexed SAED pattern, the lattice planes of $(222)_{YO}$ and $(\bar{2}22)_{YO}$ are almost parallel to those of $(\bar{2}12)_{NYF}$ and $(\bar{2}\bar{1}0)_{NYF}$, respectively. The 3.06 nm of lattice spacings of $(222)_{YO}$ is about double that of 1.518 nm for $(\bar{2}12)_{NYF}$, whereas the 3.06 nm of $(\bar{2}22)_{YO}$ is 1.5 times that of 1.951 nm for $(\bar{2}\bar{1}0)_{NYF}$. Because of such a structural relationship between Y_2O_3 and β-$NaYF_4$ (see the Supporting Information, Figure S13), the zone axis of $[1\bar{2}2]$ of β-$NaYF_4$ inherits that of $[0\bar{1}1]$ of Y_2O_3, implying a possible epitaxial nucleation of β-$NaYF_4$ on some specific Y_2O_3 surfaces can take place. This structural relationship is schematically illustrated in the Supporting Information, Figure S13. If this model is correct, the barrier energy for the nucleation of β-$NaYF_4$ should be markedly reduced and fully explains the growth of β-$NaYF_4$ with no formation of an intermediate α-$NaYF_4$ phase. TEM imaging of pure phase β-$NaYF_4$ product particles (c and d in Figure 6) indicates that the porous structure of topotactic nanoparticles may be initially retained (Figure 6c), but with further growth and aging much larger less defective single crystals have been formed (Figure 6d) implying both interior and exterior growth for the initially formed smaller porous grains.

Photoluminescence Properties of β-$NaYF_4$:Eu^{3+} Microcrystals. A variety of groups reported the preparation of $NaYF_4$:Eu^{3+} nano- and microcrystals and the measurement of the excitation and emission spectra.[21,23] Because both β-$NaYF_4$ and β-$NaEuF_4$ could be prepared phase pure by our methodology, a solid solution is then prepared with 5% doping of Eu in the Y site. Figure 7 and the Supporting Information, Figure S14, show the excitation and emission spectra of the $NaYF_4$:$0.05Eu^{3+}$ microdisks grown from ethanol, *n*-butanol, and *n*-hexanol. Monitoring the emission at 617 nm, the excitation spectrum consists of many sharp

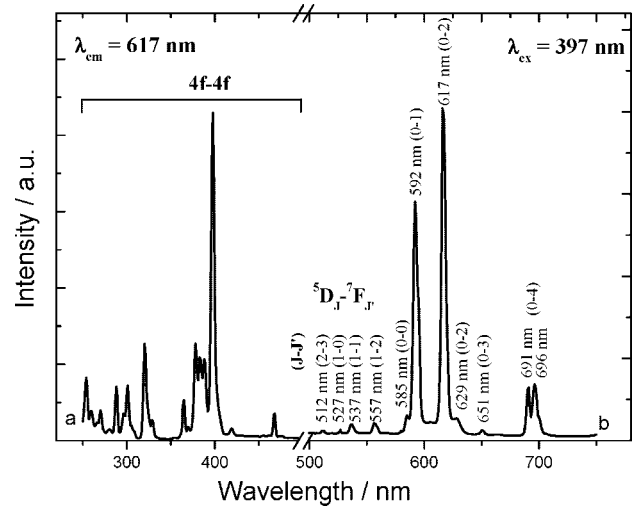

Figure 7. Excitation (λ_{em} = 617 nm) and emission (λ_{ex} = 397 nm) spectra of β-$NaYF_4$:$0.05Eu^{3+}$ synthesized in ethanol at 220 °C for 24 h.

peaks, due to the characteristic 4f−4f transitions of Eu^{3+} from the ground state $^7F_0$ to the excited levels. The strongest excitation peak at 397 nm is assigned to the transition of $^7F_0 \rightarrow {}^5L_6$.

The Eu^{3+} ions can be used to examine the presence of oxygen in fluoride materials, because the charge transfer band (CTB) of $O^{2-}-Eu^{3+}$ is very sensitive to a trace of oxygen impurity. For example in $NaGdF_4$:Eu^{3+}, which has a fluorite-related structure, an intense broad CTB of $O^{2-}-Eu^{3+}$ was observed at 250 nm because of the presence of trace amounts of oxygen.[31] In the present case, the complete absence of this CTB indicates an extremely high purity of the fluoride products. The charge transfer band of $F^- - Eu^{3+}$ is usually located at vacuum ultraviolet region (<200 nm), which is beyond our instrumental detection range.[31] In addition, the emission of Eu^{3+} can be used as a probe to investigate its coordination environment. Using an excitation wavelength of 397 nm, there are many emission peaks due to the transitions from the excited state $^5D_{J=2,1,0}$ to the ground state $^7F_{J=0,1,2,3,4}$.[32] The emissions at 592 and 617 nm are predominant. For europium, the $^5D_0 \rightarrow {}^7F_1$ (592 nm) transition is magnetically allowed [a magnetic-dipole (MD) transition], whereas the $^5D_0 \rightarrow {}^7F_2$ (617 nm) is a hypersensitive forced electric-dipole (ED) transition that is allowed only at low symmetries. It has been extensively reported that the emission line corresponding to $^5D_0 \rightarrow {}^7F_2$ (ED) is more intense than that of $^5D_0 \rightarrow {}^7F_1$ (MD) for nano- and micrograins.[23,33] Herein, the ED transition is relatively significant as compared to MD one, indicating that the doped Eu^{3+} ions are located in a noncentrosymmetric site.[33]

The fluorescence lifetime of doped Eu^{3+} ion varies with the host material and is an important factor for many consequent applications.[23,33] Figure 8 shows the Eu^{3+} fluorescent lifetimes for β-$NaYF_4$:Eu^{3+} microcrystals grown at different temperatures in a variety of reaction media. Details are shown in the

(31) You, F. T.; Wang, Y. X.; Lin, J. H.; Tao, Y. *J. Alloys Compd.* **2002**, *343*, 151.
(32) Yu, M.; Lin, J.; Wang, S. B. *Appl. Phys. A: Mater. Sci. Process.* **2005**, *80*, 353.
(33) Ghosh, P.; Patra, A. *J. Phys. Chem. C* **2008**, *112*, 3223.

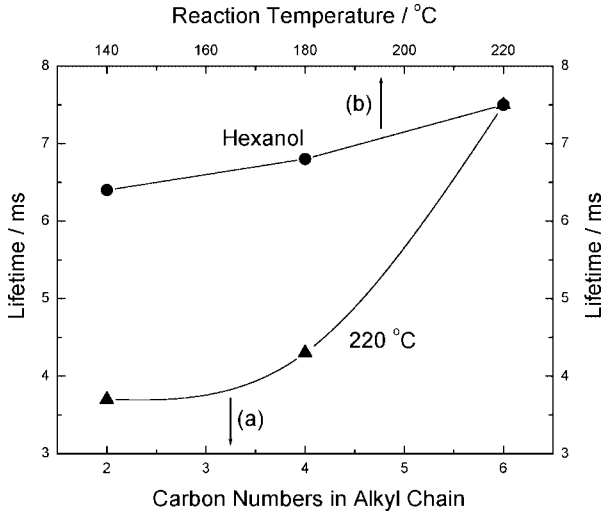

Figure 8. Dependence of lifetime ($^5D_0 \rightarrow {}^7F_2$ transition) of Eu^{3+} ions doping in β-$NaYF_4$ derived from (a) different solvents at 220 °C and (b) *n*-hexanol at different temperatures.

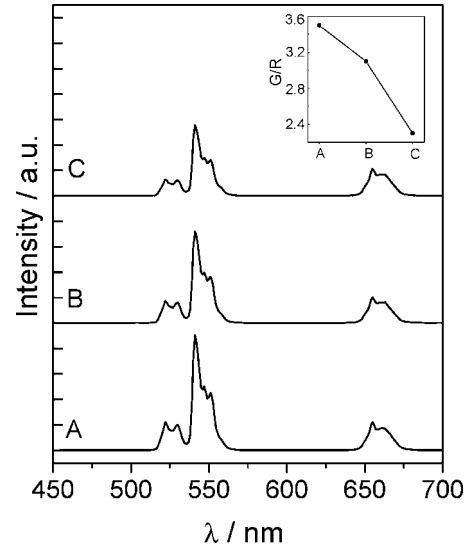

Figure 9. Up-conversion emission spectra of $NaYF_4$:Yb^{3+}/Er^{3+} crystals under NIR excitation (λ_{ex} = 980 nm). The samples were grown at 220 °C for 24 h in different solvents: (A) ethanol, (B) *n*-butanol, and (C) *n*-hexanol. The inset indicates the G/R (green versus red) ratios.

Supporting Information, Figure S15. All the curves show a single exponential decay: $I(t) = I_0\exp(-t/\tau)$, where I_0 is the luminescence intensity at $t = 0$, and τ is the lifetime. It implies that the lifetimes of Eu^{3+} ions are dependent on the morphology of the resultant microdisks, which, as we have described above, can be tightly controlled by synthetic conditions (Figure 8). τ is determined to be 3.7, 4.3, and 7.5 ms for the products synthesized from ethanol, *n*-butanol, and *n*-hexanol at 220 °C for 24 h (Figure 8a). There is evidence of a slight increase from 6.4 and 6.8 to 7.5 ms for the products from hexanol and 24 h at 140 and 180 to 220 °C, respectively (Figure 8b). Generally, the lifetime τ, which is related to both the radiative and nonradiative processes, becomes shorter in the presence of defect, because of the increase in nonradiation probability.[34] As discussed above, the size of β-$NaYF_4$ particles increases with increasing temperature and with higher alcohols. The lower specific surface area results in the decrease of defect amounts and finally in the increase of the lifetime of Eu^{3+}. It is worth noting that this facile synthesis route is ideally suited to control both of the optical properties and morphology of $NaYF_4$:Eu^{3+}. The modification of lifetime with the variation of synthesis condition and resultant crystal geometries might open a new way to optimal luminescence materials.

Photoluminescence Properties of β-$NaYF_4$:Yb^{3+}/Er^{3+} Microcrystals. To investigate the up-conversion (UC) property of these β-$NaYF_4$ hosts, 20% Yb and 2% Er were added to form codoped β-$NaYF_4$:Yb^{3+}/Er^{3+} crystals in a variety of solvents. Figure 9 shows the emission spectra of the $NaYF_4$:Yb^{3+}/Er^{3+} products. Using a 980 nm excitation as a pump, an intense green light can be observed even with the naked eyes for these size-tunable β-$NaYF_4$ crystals. The intense green emissions in the range of 510−560 nm are ascribed to Er^{3+} $^2H_{11/2} \rightarrow {}^4I_{15/2}$ and $^4S_{3/2} \rightarrow {}^4I_{15/2}$ transitions respectively and red emission in the range of 640−670 nm is ascribed to Er^{3+} $^4F_{9/2} \rightarrow {}^4I_{15/2}$. Detailed description about the up-conversion mechanism has been given in many previous reports.[18−20,22]

It has been extensively mentioned before that the UC emission features such as intensity and green to red ratio ($f_{g/r}$) are related to both the phase type and dimensions of the $NaYF_4$ host crystals.[15,19] For β-$NaYF_4$:Yb^{3+}/Er^{3+} nanocrystals with size below 70 nm, the $f_{g/r}$ decreases along with the size of the nanocrystals.[19] In the present work, the UC emissions can be modified with the change of the alcohol reaction medium (Figure 9). The values of $f_{g/r}$ are found to be 3.5, 3.1, and 2.3, respectively, when ethanol, *n*-butanol and *n*-hexanol were used as solvents and the reactions were performed for 24 h at 220 °C (Figure 9). That is, the $f_{g/r}$ of β-$NaYF_4$:Yb^{3+}/Er^{3+} decreases with the carbon number of solvent alcohol. The higher $f_{g/r}$ indicates that the Er^{3+} excited levels of $^2H_{11/2}$ and $^4S_{3/2}$ are mainly populated according to the energy level diagram and proposed UC process (see the Supporting Information, Figure S16). The decrease in the ratio of $f_{g/r}$ might be due to an increase in the nonradiative transition probability of $^2H_{11/2} \rightarrow {}^4F_{9/2}$ and $^4S_{3/2} \rightarrow {}^4F_{9/2}$, which is correlated with different surface chemistry induced by different solvents.[19] Besides the $f_{g/r}$ decreases (Figure 9, inset), UC emission intensity (I_{UC}) does so slightly. Therefore, the UC emission parameters such as I_{UC} and $f_{g/r}$ could be tuned by modifying the growth conditions and related microstructures.

Conclusion

In summary we have described the facile phase-pure solvothermal preparation of β-$NaYF_4$ directly from yttria precursor, through addition of a stoichiometric excess of a combination of sodium and ammonium hydrogen fluorides. While a variety of solvents can be used, alcohols afford the best results and the morphology and particle size of the products are controllable and well-defined. From ethanol microdisks of ca. 2 μm are formed, these

(34) Zhang, Q.; Wang, J.; Zhang, M.; Ding, W.; Su, Q. *Appl. Phys. A: Mater. Sci. Process.* **2007**, *88*, 805.

may become increasingly elongated along the hexagonal *c*-axis through use of longer chain alcohols, such as *n*-butanol or *n*-hexanol, as the reaction media. Detailed TEM studies indicate a novel match of lattice planes of the yttria precursor grains and product β-$NaYF_4$ and indicate the possibility of topotactic growth. This may circumvent formation of cubic α-$NaYF_4$ phase commonly seen in such syntheses as an intermediate. The PL properties of both Eu^{3+} and Yb^{3+}/Er^{3+} doped β-$NaYF_4$ microdisks have been investigated and important features such as fluorescent lifetime and green-red ratio for UC have been found to be dependent on the size and morphology of the microdisks. The results from this system underline the important role that controlled morphological syntheses can play in optimizing key properties of advanced functional materials.

Acknowledgment. This work has been supported financially from National Natural Science Foundation (NSF) of China and the Government of Guangdong Province for NSF (U0734002, 20571087, and 5003273). We are grateful to Prof. Jianying Zhou at the Laser and Spectroscopy Institute in our University for helpful discussions.

Supporting Information Available: Additional figures (PDF). This material is available free of charge via the Internet at http://pubs.acs.org.

CM802543K